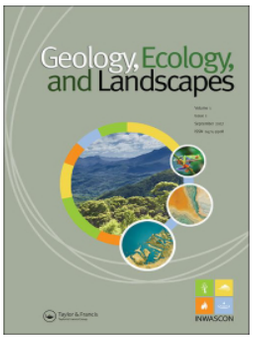

Geology, Ecology, and Landscapes

ISSN: (Print) (Online) Journal homepage: www.tandfonline.com/journals/tgel20

Seasonal and annual trends in reference evapotranspiration and prediction using machine learning models across seven climatic zones of Bangladesh

Md. Naimur Rahman

To cite this article: Md. Naimur Rahman (13 Nov 2024): Seasonal and annual trends in reference evapotranspiration and prediction using machine learning models across seven climatic zones of Bangladesh, Geology, Ecology, and Landscapes, DOI: 10.1080/24749508.2024.2429223

To link to this article: https://doi.org/10.1080/24749508.2024.2429223

Published online: 13 Nov 2024.

GEOLOGY, ECOLOGY, AND LANDSCAPES
https://doi.org/10.1080/24749508.2024.2429223

RESEARCH ARTICLE

OPEN ACCESS Check for updates

Seasonal and annual trends in reference evapotranspiration and prediction using machine learning models across seven climatic zones of Bangladesh

Md. Naimur Rahman [a,b,c]

[a]Department of Geography, Hong Kong Baptist University, Hong Kong, China; [b]David C Lam Institute for East-West Studies, Hong Kong Baptist University, Hong Kong, China; [c]Department of Development Studies, Daffodil International University, Dhaka, Bangladesh

ABSTRACT

The primary aim of this investigation is to examine the historical (1989–2020) and future trends and magnitude of Reference Evapotranspiration (ET_0) in terms of spatiotemporal measures, considering its significance as a hydro-meteorological parameter influenced by changing climate. The FAO-56 Penman-Monteith method is employed to analyze ET_0, while the Modified Mann Kendall test is utilized to assess trends and Sen's Slope Estimator is used for magnitude analysis. The future prediction is conducted using Support Vector Machine (SVM), Artificial Neural Network (ANN), and Random Forest (RF) models. Results show an increasing ET_0 trend annually in the southeastern and northeastern zones, while decreased values are observed in other regions, particularly in the northwest (0.83 mm). Sen's slope estimator reveals distinct fluctuations in ET_0, with notable disparities in the Southeastern, Northeastern, Southwestern, and South-Central zones. Notably, Chattogram and Sitakunda experience an ET_0 magnitude of 0.02 mm/Year, while other zones show a magnitude of 0.01 mm/Year. SVM outperformed other models, predicting rising ET_0 in various seasons. These findings offer insights for optimizing irrigation systems and sustainable water management under changing climatic conditions.

ARTICLE HISTORY
Received 11 October 2023
Accepted 10 November 2024

KEYWORDS
Reference evapotranspiration; Bangladesh; machine learning; spatial

1. Introduction

The evaluation of ET_0 holds critical significance in the efficient management and design of agricultural hydrology, the formulation of ideal irrigation scheduling strategies, and the creation of models for optimizing crop growth (Pereira et al., 2020; Salam, Towfiqul Islam, et al., 2020). ET_0, situated at the intersection of hydrological and carbon cycles, is intricately linked to crop yield and energy balance. Furthermore, its effects resonate through ocean-atmospheric circulation systems, significantly impacting climatic variations (Fan et al., 2019; Jung et al., 2010). Accurate assessment of ET_0 enables agricultural decision-makers to make well-informed choices, promoting sustainable practices and effective resource management (Behboudian et al., 2021). ET_0 is governed by many environmental parameters, including wind speed, relative humidity, air temperature, solar radiation (SR), and sunshine duration (SD), all of which intricately interplay to influence its dynamics (Rajput et al., 2024). Understanding the variations in ET_0 has proven to be challenging due to unpredictable fluctuations in these climatic factors. Surprisingly, despite a clear link between ET_0 and temperature, divergent trends have been observed in different regions of the earth. The "evapotranspiration paradox" is a global phenomenon affecting numerous regions, with extensive research identifying the primary contributing factors as decreasing SD and declining wind speeds (Fu et al., 2022; Kitsara et al., 2013; Wang et al., 2014; Xing et al., 2016).

The phenomenon of climate change has enhanced the atmosphere's capacity to retain moisture, leading to increased cloud formation and a subsequent reduction in SD and SR across various regions (Mishra, 2019). It is important to note that the impact of increased cloud cover on SD and SR varies depending on the type of clouds present (Matuszko, 2012). Additionally, regional variability in cloud cover changes has been significant. For example, cloud cover has markedly increased in Southeast Asia, while it has decreased in North America (Dai, 2021; Mao et al., 2019). Similar variability has been observed in other meteorological factors, such as relative humidity, which increased by up to 2.0% per decade over the past four decades in key regions of the United States, China, and India while remaining relatively stable in other areas (Mao et al., 2019).

Furthermore, wide-ranging fluctuations in meteorological conditions have led to notable disparities in ET_0 trends across various regions (Cabral Júnior et al., 2019; Chen et al., 2023; Ndiaye et al., 2020; Ramachandra et al., 2022) Reports of ET_0 trends from various regions highlight the heterogeneity in its behavior. Notably, substantial increases in ET_0

CONTACT Md. Naimur Rahman naimurbrur@gmail.com; naimurbrur@life.hkbu.edu.hk Department of Geography, Hong Kong Baptist University, Kowloon Tong, Hong Kong 999077, China

were reported in China (Chen et al., 2023; Dong et al., 2020), Egypt (Yassen et al., 2020), U.S.A. (McEvoy et al., 2020), Senegal (Ndiaye et al., 2020), Iran (Biazar et al., 2019; Dinpashoh & Babamiri, 2020), India (Baruah et al., 2023; Ramachandra et al., 2022) and Pakistan (Ahmad et al., 2021; Ashraf et al., 2023). Conversely, reductions in ET_0 were observed in Iran (Cheshmberah & Zolfaghari, 2019) and Brazil (Cabral Júnior et al., 2019; Ferreira et al., 2022). Some areas, such as Peninsula Malaysia (Pour et al., 2020) and the Mountains of Qilian in China (Lin et al., 2018), have shown no significant variation in ET_0. In certain regions increasing and decreasing trends in ET_0 were reported, as observed in the Tibetan Highland (Zhang et al., 2019) and the Huahe River basin (Li et al., 2018).

For a tropical, humid country like Bangladesh, predominantly situated in deltas, understanding the relationship between ET_0 and other climatic variables presents a complex challenge (Jerin et al., 2021). Changes in ET_0 can substantially influence crop yield, land suitability, and irrigation demand in this agriculturally dependent region (Katerji & Rana, 2011; Wang et al., 2017). Moreover, ET_0 plays a critical role in managing several hydrological risks that directly or indirectly impact this highly vulnerable nation, including droughts, soil salinization, low river flows, and groundwater depletion (Kamruzzaman et al., 2019; Mainuddin et al., 2015; Rahman et al., 2021). It is imperative to closely monitor and conduct comprehensive analyses since even a minor change in ET_0 can significantly impact the ecology and ecosystem of the nation (Jerin et al., 2021).

With evident patterns of rising temperatures across the nation, the effects of climate change in Bangladesh have become more pronounced (Rahman et al., 2023). Reports of variations in precipitation patterns, particularly during the monsoon and pre-monsoon seasons, have also emerged (Rahman & Azim, 2021b). Various other meteorological factors have changed as a result of global warming and other environmental shifts (Hwang et al., 2020; Rahman and Azim, 2022). For instance, the hours of sunshine have significantly decreased due to increased air pollution (Rahman et al., 2023). ET_0 in Bangladesh has unavoidably been impacted by these climate changes (Rahman et al., 2023). To understand the impact of climate change on ET_0, it is crucial to explore the spatiotemporal trend and magnitude in the context of Bangladesh. At present, only two notable studies have been identified in the literature, each with a distinct focus. Jerin et al. (2021) emphasized spatiotemporal evaluation, while Salam, Islam, et al. (2020) focused primarily on methodological approaches. However, both studies were limited by insufficient station coverage and restricted applicability across Bangladesh's seven climatic zones. Against this backdrop, the current research offers a significant contribution.

This study seeks to address the existing research gap regarding the spatiotemporal trends, magnitude evaluation, and prediction of evapotranspiration (ET_0) in Bangladesh. Among the various methods for estimating evapotranspiration, this research employs the FAO-56 Penman-Monteith method, which is a fully physically based model that incorporates principles of mass and energy conservation (FAO, 2024). This method is widely regarded as a benchmark for estimating reference evapotranspiration in numerous studies, underscoring its efficacy as an estimation technique (Sahoo et al., 2012; Srivastava et al., 2018). In addition to the FAO-56 Penman-Monteith method for estimation, the study utilizes several machine learning models for predictive purposes, demonstrating improved results across seven climatic zones in the country (Ikram et al., 2023; Kumari et al., 2022). This innovative approach sets this study apart from previous research by integrating machine learning models and achieving a more comprehensive coverage of stations and climatic zones, which has not been accomplished before.

The primary objective of this study is to provide comprehensive insights into the evolving dynamics of ET_0 (or potential evapotranspiration) in Bangladesh. By analyzing existing data and trends, the research will illuminate the underlying patterns and factors contributing to fluctuations in ET_0 over time. The findings hold significant value for various sectors, including agriculture, hydrology, and resource management. Ultimately, this research will equip decision-makers with the information necessary to make informed choices regarding crop selection, irrigation schedules, water resource allocation, and other critical operational aspects. Moreover, the study will also help identify adaptation strategies and measures to mitigate the impacts of climate change on the country's water resources and agricultural productivity.

2. Materials and methods

2.1. Study area

Bangladesh covers an area of roughly 147,610 square kilometers and is located within the geographic coordinates of 20°34 N to 26°38 N latitude and 88°10 E to 92°41 E longitude. It is the world's biggest deltaic nation in the Ganges-Brahmaputra-Meghna (GBM) river basin. Bangladesh's climatic cycles are distinguished by several seasons, notably the pre-monsoon period from March to May, the monsoon period from June to August, the post-monsoon period from September to November, and the winter period from December to February. As shown in Figure 1, these seasons outline seven unique climatic zones across the country: the southeastern area (A), the northeastern region (B), the northern section of the northern region

(C), the northwestern region (D), the western region (E), and the southwestern region (F) and south-central region (G). The climate of Bangladesh is classified as subtropical humid monsoonal, typified by the influence of the monsoon winds. Notably, the northwestern segment of the nation encounters recurrent drought conditions owing to insufficient water resources, leading to an annual mean rainfall of less than 1200 mm (M. Rahman et al., 2021; Rahman & Azim, 2022). Therefore, the southeastern and northeastern zones have high rainfall intensity (Rahman & Azim, 2022). Consequently, the western part of

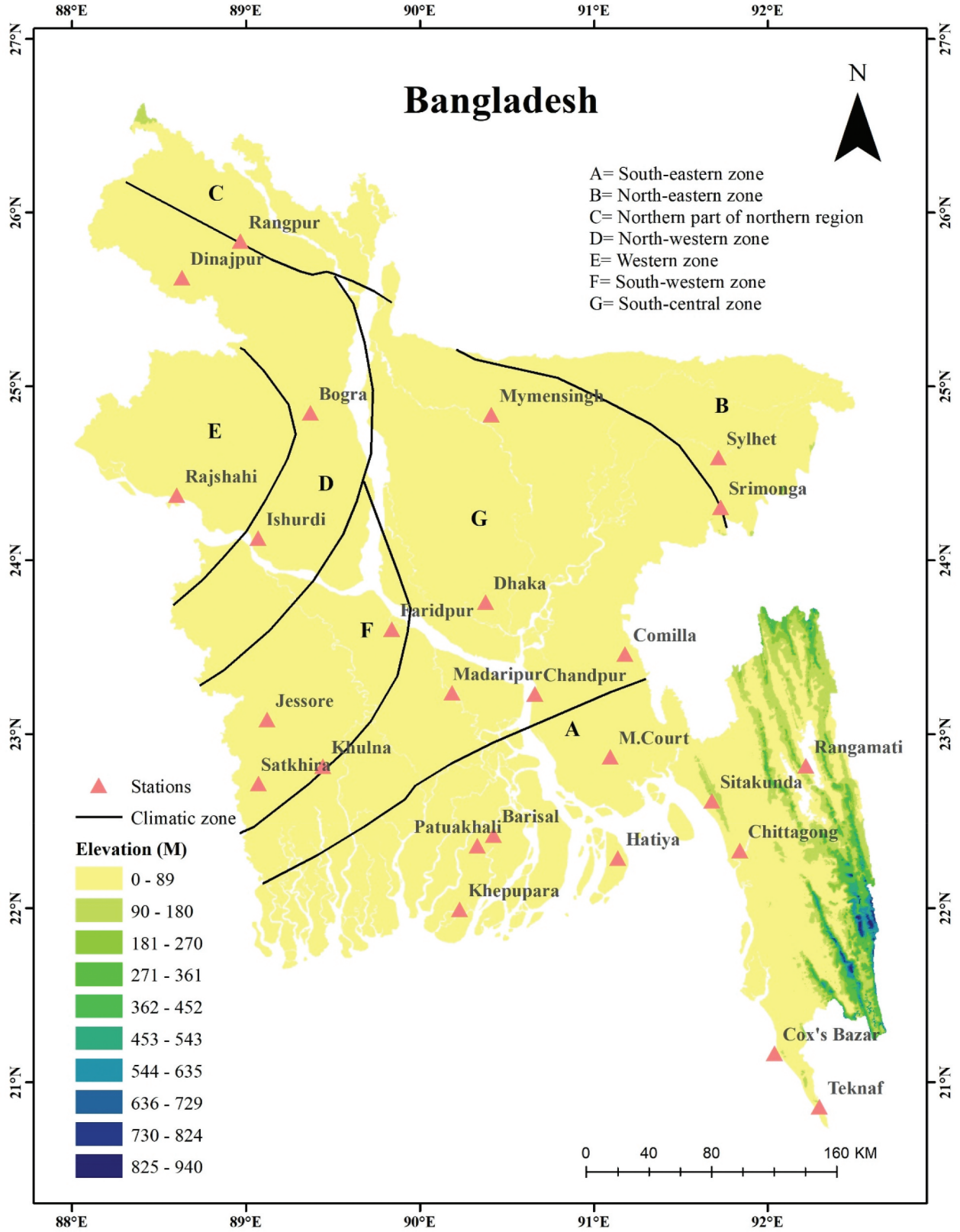

Figure 1. Demonstrate the digital elevation model of seven climatic zones of Bangladesh.

Bangladesh consistently exhibits drier climatic conditions compared to other regions. Figure 1 shows the study area of this research (M. Rahman et al., 2021; Rahman & Azim, 2022).

2.2. Data analysis and pre-processing

Maximum temperature, minimum temperature, atmospheric humidity, wind velocity, and sunshine information originating from 26 research locations under the purview of the Bangladesh Agricultural Research Council (BARC) were systematically compiled spanning the period of 1989 to 2020. The incidence of absent data was minimal, accounting for less than 2% of the dataset, thereby facilitating the uninterrupted progression of the meteorological investigation (M. N. Rahman & Azim, 2021a). For testing the homogeneity, the von Neumann ratio, standard normal homogeneity test, and range test were tested, and the datasets were found to be homogeneous (Alexandersson, 1986; Buishand, 1982). Hence, for the prediction study, 70% of the data were used for training, and the rest 30% of the data was used for testing.

2.3. Methods

To explore the seasonal and annual variations in ET_0, this research utilized the Modified Mann-Kendall (MMK) trend test (Kendall, 1975; Mann, 1945). This test allowed for the assessment of trends over time, indicating potential changes in ET_0. Consequently, the author employed Sen's Slope Estimator (Sen, 1968) to quantify the magnitude of ET_0 based on the identified trends. Subsequently, the FAO-56 Penman-Monteith method was utilized to extract ET_0 values, leveraging available climatological data, including solar radiation, air temperature, humidity, and wind speed (Batchelor & Roberts, 1983; Bernadette et al., 2014) (Figure 2). This method is considered a benchmark for estimating ET0 due to its comprehensive approach that accounts for the combined effects of these climatic parameters.

In addition to these methods, the author applied machine learning models, including ANN, SVM, and RF, to predict future variations in ET_0. These models are well-established in the field of predictive analytics, offering significant advantages in accuracy for various forecasting purposes (Elbeltagi et al., 2021; Heramb et al., 2023). By integrating historical data, we ensured a robust framework for our predictions, while being mindful of potential missing values, which typically do not exceed 2% to maintain the integrity of the analysis (Mortuza et al., 2019; Rahman et al., 2021).

2.3.1. ET_0 estimation

The FAO Penman-Monteith equation leverages available climatological data, including solar radiation, air temperature, humidity, and wind speed (Batchelor & Roberts, 1983; Bernadette et al., 2014). Higher temperatures and solar radiation increase ET_0 by providing more energy for vaporization. Wind speed enhances ET_0 by reducing the boundary layer's thickness, facilitating water vapor transport. Humidity influences ET_0 through the vapor pressure deficit: lower humidity increases ET_0 by creating a larger deficit, while higher humidity decreases ET_0 by reducing the deficit (Batchelor & Roberts, 1983; Bernadette et al., 2014; FAO, 2024). This model ensures a comprehensive ET_0 estimate by considering these parameters collectively. Ideally, these weather measurements should be collected 2 meters above a well-watered, extensive green grass surface (Batchelor & Roberts, 1983; Bernadette et al., 2014). This study opted to estimate ET_0 using the FAO56-PM recommended equation based on existing meteorological data rather than relying on ET_0 measurements obtained from an evaporation pan. The FAO56-PM equation, proposed by (Allen et al., 1998), is widely recognized as the global standard model for estimating ET_0. The equation itself is expressed as:

$$ET_0 = \frac{0.408\Delta(R_n - G) + \gamma \frac{900}{T+273} U_2(e_s - e_a)}{\Delta + \gamma(1 + 0.34U_2)} \quad (1)$$

Here, ET_0 is reference evapotranspiration (mmd^{-1}), is net radiation at the crop surface ($MJm^{-2}\ d^{-1}$), G is soil heat flux density ($MJm^{-2}\ d^{-1}$), T is the mean daily air temperature at 2 m height (°C), is wind U_2 speed at 2 m height (ms^{-1}), e_s is saturation vapour pressure (kPa), e_a is actual vapour pressure (kPa), $e_s - e_a$is saturation vapour pressure deficit (kPa), the slope of vapour pressure curve (kPa °C Δ is – 1), γ is psychrometric constant (kPa °C-1), recommended G = 0 (Allen et al., 1998).

2.3.2. ET_0 prediction

ANN, SVM, and RF were employed to see the future variabilities of ET_0. These methods are widely accepted as prediction models for different prediction purposes, and predicting ET_0 is one of them (Elbeltagi et al., 2021; Heramb et al., 2023). Incorporating historical data is a valuable practice, but one must beware of missing data. Typically, a missing value of up to 2% is considered acceptable, as it has a relatively low impact on outcomes and is highly unlikely to have any significant influence on the results (Mortuza et al., 2019; Rahman et al., 2021).

In this study, the input variables for the prediction model included maximum and minimum temperature, sunshine, humidity, and wind speed (Figure 2). To train and validate the model, we utilized historical climate data spanning from 1989 to 2020, collected from 26 meteorological stations. The dataset was divided into two portions, with 70% allocated for

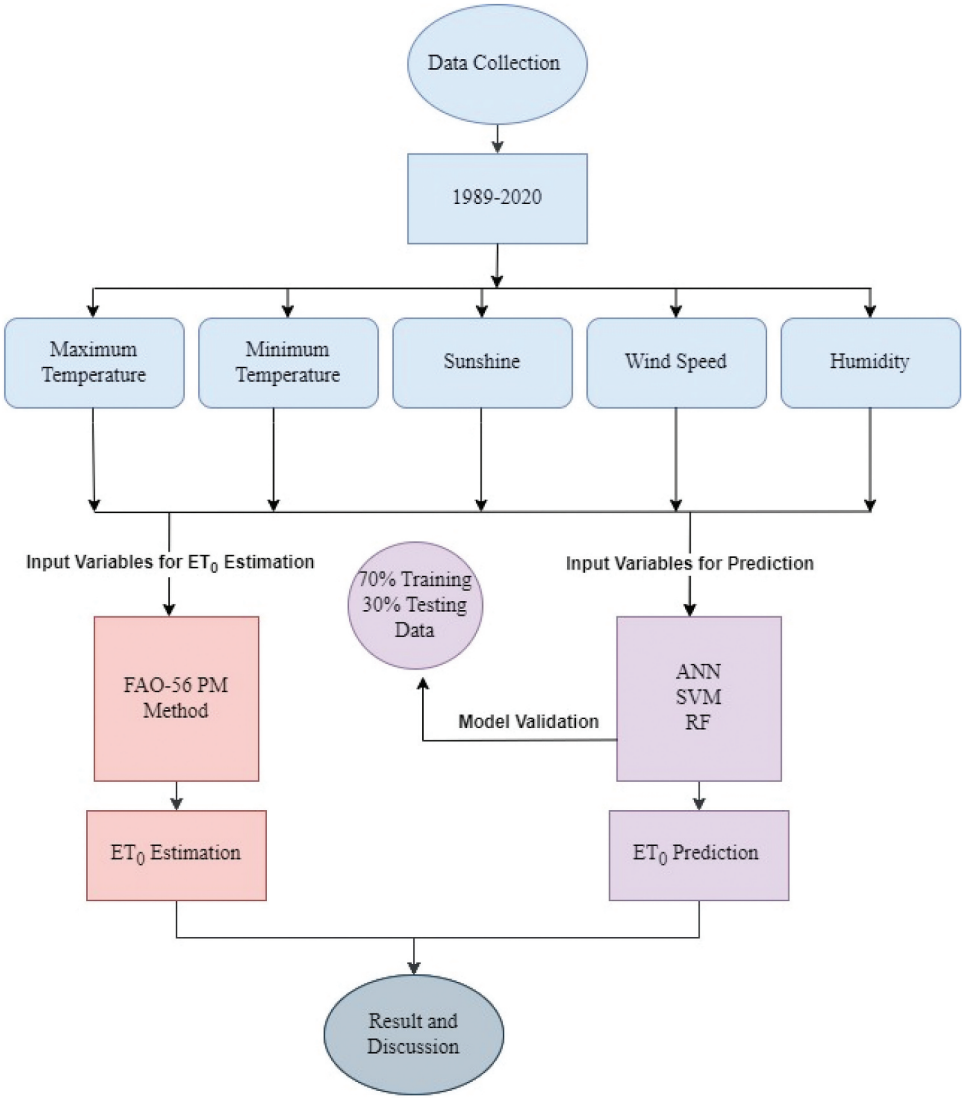

Figure 2. Comprehensive overview of the research design framework.

training and 30% for testing, ensuring robust model validation. Predictions generated by ANN, SVM, and RF were assessed using statistical metrics such as Root Mean Square Error (RMSE), Mean Absolute Error (MAE), and the Coefficient of Determination (R^2)

The ANN is a highly advanced form of Artificial Intelligence that is specifically designed to simulate the complex biological neural networks of the human brain (Azid et al., 2013; Moustris et al., 2010). ANN can learn and recognize intricate patterns to make predictions, classify data, and cluster. ANN has become extremely popular due to its exceptional accuracy in making predictions, the advanced algorithms employed, and highly sophisticated techniques (Azid et al., 2014; Chaloulakou et al., 2003).

The SVM is an incredibly effective and widely used machine learning algorithm, ideal for classification and regression analysis tasks. This type of supervised machine learning algorithm is specifically designed to identify the optimal hyperplane in a given dataset, ensuring that different classes are effectively separated (Meris et al., 2020; Salam & Islam, 2020).

RF is an exceptional tree-based supervised ensemble learning model proposed by Breiman (2001) that has revolutionized the field of machine learning. Breiman's contribution was to improve the Bagging models to RF, which is now widely used for predicting as well as regression problems. It is a highly sophisticated yet simple and robust model that offers remarkable prediction accuracy, making it a clear winner when compared to the Adaboost. The error produced by RF is dependent on individual trees, and the model trains various decision trees from two viewpoints: one is the sample dimension, and the other one is the feature dimension. With its unique features and unparalleled accuracy, Random Forest is undoubtedly the go-to model for various complex machine-learning challenges (Dong et al., 2020).

Three commonly used statistical indicators (Quej et al., 2019) were used to evaluate and compare the accuracy and performance of the studied models for daily ET_0 estimation: coefficient of determination (R^2, Equation (2)), root mean square error (RMSE, Equation (3)), and mean absolute error (MAE,

Equation (4)). The statistical indicators' mathematical equations are:

$$R^2 = \frac{\sum_{i=1}^{n}\left(Y_{i,m} - Y_{i,e}\right)^2}{\sum_{i=1}^{n}\left(Y_{i,m} - \bar{Y}_{i,e}\right)^2} \quad (2)$$

$$RMSE = \sqrt{\frac{1}{n}\sum_{i=1}^{n}\left(Y_{i,m} - Y_{i,e}\right)^2} \quad (3)$$

$$MAE = \frac{1}{n}\sum_{i=1}^{n}\left|Y_{i,m} - Y_{i,e}\right| \quad (4)$$

$$MSE = \frac{1}{n}\sum_{i=1}^{n}\left(Y_{i,m} - \hat{Y}_{i,e}\right)^2 \quad (5)$$

where Yi,m, Yi,e, $\bar{Y}_{i,e}$ and n is the measured, estimated, and mean of global solar radiation, respectively, and n is the number of observations. Higher R^2 values, i.e., closer to 1, indicate higher model performance and a regression line that fits the data well. The lower the RMSE and MAE values, the better the model performs.

2.3.3. ET_0 spatial interpolation

In this study, the Inverse Distance Weighting (IDW) method was employed as a reliable and widely used interpolation technique to estimate unknown hydrological or geographic values (Amini et al., 2019; Das, 2019). This approach operates on the principle that each known data point exerts an influence on its surroundings, which diminishes as the distance from the point increases (Ozelkan et al., 2015). The weight assigned to each point is inversely proportional to its distance from the location of interest, providing an accurate estimation based on proximity (Hodam et al., 2017). IDW was chosen for its simplicity and effectiveness in capturing local spatial variability(Rahman et al., 2023).

3. Result and discussion

3.1. Trend and magnitude of ET_0

The topographical variation in the trend of ET_0 (Figure 3) reveals a declining prevalence of adverse trends in the northwestern, western, southwestern, and south-central regions during the pre-monsoon season. In contrast, the northern section of the northern region exhibits a significant negative trend, with a Z-statistic of − 3.84 (Figure 3). Conversely, the southeastern, northeastern, and parts of the south-central zones show a positive trend in ET_0 (Figure 3). Additionally, the magnitude of the ET_0 pattern shows negative slope values in the northern part of the northern region, as well as in the northwestern and southwestern zones, which aligns with the Modified Mann-Kendall trend findings presented in Table 1. On the other hand, several scattered locations in the southeastern and northeastern zones exhibit a significant ET_0 magnitude of 0.02, as shown in Table 1.

During the monsoon season, all zones and stations display positive trends, except specific areas: the northern section of the northern region (Rangpur), the northwestern region (Bogura and Dinajpur), and the southeastern zone (Hatiya) (Figure 3). Among these zones, the northern part of the northern region stands out with the most pronounced negative trend, indicated by a Z-statistic of less than − 4.70 (Figure 3). In contrast, Sen's slope estimation indicates positive or negligible magnitudes in several areas across all zones, except for the northern part of the northern region, as presented in Table 1. Furthermore, the northern part of the northern zone shows a substantial negative ET_0 value of −0.02 mm/year (Table 1).

In the post-monsoon season, a positive ET_0 trend is observed across all zones, except three specific stations: Rangpur (−0.52 Z statistic), Satkhira (−0.032 Z statistic), and Madaripur (−0.032 Z statistic). These stations are in the northern part of the northern region, the southwestern zone, and the south-central zone, respectively (Figure 3). Notably, the most significant positive trends are recorded in Sitakunda (Z = 4.53), Patuakhali (Z = 4.13), and Sylhet (Z = 4.13), covering the southeastern and northeastern zones, as shown in the map. The magnitude of ET_0 changes remains relatively consistent, except in Chattogram and Sitakunda, where a slight increase of 0.02 mm/year is observed in the southeastern zone (Table 1).

All zones, except the southeastern, northeastern, and northern parts of the northern region, show a significant decline in the ET_0 trend in the winter season. Only one point in the southwestern and south-central zones exhibits an increasing trend (Figure 3). The most pronounced positive trends are concentrated in the southeastern and northeastern zones, particularly at Sitakunda (Z = 4.63), Patuakhali (Z = 3.85), and Chattogram (Z = 3.53) in the southeastern zone, and Srimangal (Z = 3.54) and Sylhet (Z = 3.36) in the northeastern zone, as illustrated in Figure 3. Trend variations differ considerably, with the highest variance reaching 0.04 mm/year in the southeastern zone and 0.02 mm/year in the northeastern zone (Table 1). Conversely, substantial negative trends are recorded in Rajshahi (−2.38 mm/year) in the western zone, Madaripur (−3.21 mm/year) in the south-central zone, Hatiya (−3.98 mm/year) in the southeastern zone, and Satkhira (−3.85 mm/year), Khulna (−2.48 mm/year), and Faridpur (−2.11 mm/year) in the southwestern zone, as detailed in Table 1.

The annual spatial trend analysis reveals a notably high ET_0 trend in the southeastern and northeastern zones, primarily due to their dense hilly and forested areas. In contrast, a reduced ET_0 trend is observed in the remaining climatic zones, with the northwestern

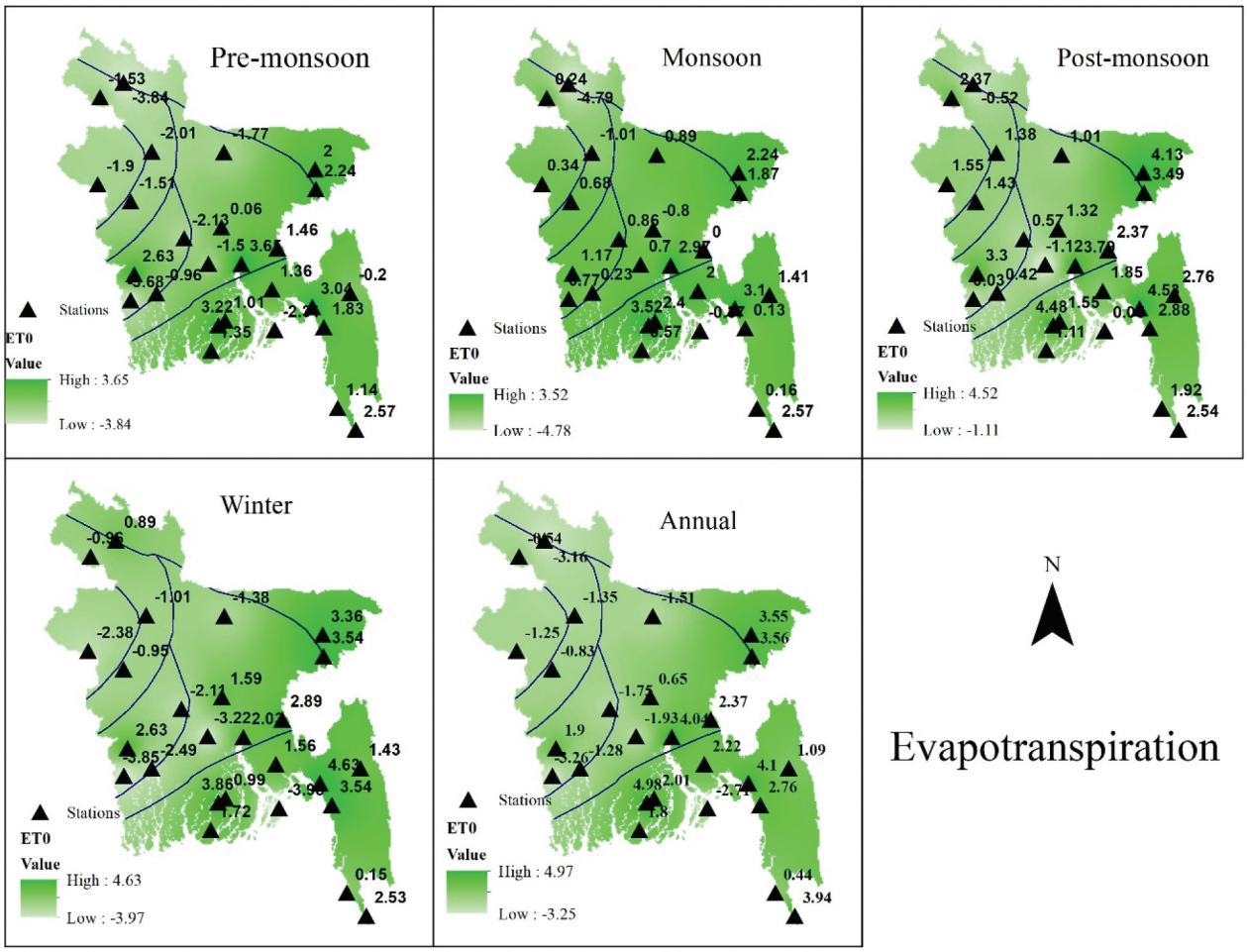

Figure 3. Demonstrates spatiotemporal distribution of ET_0 trend in sub-climatic zones at 95% confidence interval.

Table 1. Demonstrate the magnitude of the trend of ET_0, (all the values are calculated at a 95% confidence interval; bold values indicate significant increased or decreased values).

Zone	Station	Pre-monsoon	Monsoon	Post Monsoon	Winter	Annual
ET_0						
South Eastern	Khepupara	0.01	0.00	0.00	0.01	0.01
	Barisal	0.01	0.01	0.00	0.00	0.01
	Chattogram	**0.02**	0.00	**0.02**	**0.04**	**0.02**
	Cox's Bazar	0.01	0.00	0.01	0.00	0.00
	Hatiya	**−0.01**	0.00	0.00	−0.01	**−0.01**
	Sitakunda	**0.02**	0.01	**0.02**	**0.02**	**0.02**
	Teknaf	0.01	0.01	0.01	0.01	0.01
	Rangamati	0.00	0.01	0.01	0.00	0.00
	M.court	0.01	0.01	0.01	0.01	0.01
	Patuakhali	**0.02**	0.01	0.01	0.01	0.01
North Eastern	Srimangal	**0.02**	0.01	0.01	**0.02**	0.01
	Sylhet	**0.02**	0.01	0.01	**0.02**	0.01
Northern Part of Northern Region	Rangpur	**−0.02**	**−0.02**	0.00	0.00	**−0.01**
North Western Region	Ishurdi	**−0.01**	0.00	0.01	0.00	0.00
	Bogura	**−0.02**	0.00	0.01	0.00	**−0.01**
	Dinajpur	**−0.01**	0.00	0.01	0.00	0.00
Western	Rajshahi	**−0.01**	0.00	0.00	−0.01	0.00
South western	Khulna	0.00	0.00	0.00	−0.01	0.00
	Faridpur	**−0.01**	0.00	0.00	−0.01	**−0.01**
	Jashore	0.01	0.01	0.01	0.01	0.01
	Satkhira	**−0.02**	0.00	0.00	−0.02	**−0.01**
South Central	Dhaka	0.00	0.00	0.01	0.01	0.00
	Comilla	0.01	0.00	0.01	0.03	0.01
	Chandpur	**0.02**	0.02	0.01	0.01	0.01
	Madaripur	**−0.01**	0.00	0.00	−0.01	0.00
	Mymensingh	**−0.01**	0.00	0.00	−0.01	**−0.01**

zone displaying the lowest value at 0.83, as demonstrated in Figure 3. Furthermore, Sen's slope estimator demonstrates variations in the magnitude of ET_0 across different parts of the Southeastern, Northeastern, Southwestern, and Southcentral climatic zones. Specifically, Chattogram and Sitakunda exhibit an ET_0 of 0.02 mm/year, while other zones maintain a slightly lower ET_0 of 0.01 mm/year. Conversely, a significant decline in ET_0 is noted in the northern part of the northern region (−0.01 mm/year) and specific areas within the southeastern, northwestern, southwestern, and south-central zones, including Hatiya, Bogura, Faridpur, Satkhira, and Mymensingh, where ET_0 also stands at −0.01 mm/year as shown in Table 1. The observations revealed a correlation between seasonal variations in maximum and minimum temperatures. The declining trend in ET_0, representing potential evapotranspiration, aligns with the results of previous research studies. This indicates the presence of a broader underlying climatic pattern affecting plants' ability to absorb and retain moisture across various regions (Salam & Islam, 2020). This pattern is attributed to the spatiotemporal temperature variations that exist within different subclimatic zones of the country. These variations are caused by factors such as variations in altitude, the proximity to the coast, and seasonal changes. The studies indicate that while some regions of the country experience increasing temperatures and ET_0 trends, others show a decline (Kamal et al., 2021; M. N. Rahman & Azim, 2021a; M. Rahman et al., 2021)

3.2. Prediction of ET_0

This study utilizes three distinct predictive models: ANN, SVM, and RF. Assessing model accuracy is a critical phase in the development of machine learning models, as it allows for the evaluation of prediction performance. The assessment includes metrics such as MSE, MAE, RMSE, and R-squared. The dataset is split, with 70% used for training and the remaining 30% reserved for testing. Although memorization performance is considered, it is not sufficient as the sole evaluation metric. Therefore, testing results are analysed to demonstrate prediction accuracy. Negative R-squared values indicate a poor model fit; however, in this study, no negative R-squared values were observed, with a statistic of zero indicating the absence of such cases.

Zone A, located in the southeastern region, demonstrated significant performance of the SVM model, as shown in Table 2, with no zero or negative R-squared values. The RMSE values were particularly low, with measurements of 0.16, 0.04, 0.03, 0.08, and 0.15 for the pre-monsoon, monsoon, post-monsoon, winter, and annual seasons. These low RMSE, MSE, and MAE values underscore the model's accuracy. Consequently, it is anticipated that the monsoon, post-monsoon, and winter seasons will exhibit higher ET_0, with positive prediction values of 96%, 94%, and 85%, respectively. The pre-monsoon season is projected to show a 77% increase in ET_0 variation. These results align with the validation performance, further emphasizing the effectiveness of the SVM model. In contrast, the other two models showed relatively minor performance and were deemed unsuitable for Zone A.

In Zone B, encompassing the northeastern region, the ANN and RF models exhibited lower performance than the SVM model across all seasonal and annual timeframes. This is evident from the R-squared values in Table 2, where some instances even resulted in negative values or nominal predictive outcomes for ANN and RF. Conversely, the SVM model demonstrated consistently strong performance throughout all seasons. This is reflected in the low RMSE values, ranging from 0.01 (monsoon) to 0.11 (winter), with a minimum of 0.05 achieved annually. Additionally, the SVM model yielded minimal MSE values, ranging from 0.0003 (monsoon) to 0.14 (winter), and MAE values ranging from 0.01 (monsoon) to 0.08 (winter) across all seasons and annually. These findings are consistent with the validation performance, solidifying the SVM model's efficacy in Zone B. Similar to Zone A, projections for Zone B indicate a rise in potential evapotranspiration (ET_0) across all seasons. The expected increases are 97% (pre-monsoon), 99% (monsoon), 91% (post-monsoon), 74% (winter), and 91% (annual).

In Zone C, located in the northern region, the ANN model demonstrated strong performance for estimating ET_0 during the pre-monsoon, post-monsoon, and winter seasons. Notably, the post-monsoon season exhibited a significant 100% increase in ET_0, as predicted by the ANN model. R-squared values of 0.92 and 0.55 for the pre-monsoon and annual periods indicated an upward trend in ET_0. However, the ANN model's capability for predicting the RF variable during the winter season was negligible. In contrast, the SVM model achieved consistently high performance across all seasons, with R-squared values exceeding 0.87 for each period (pre-monsoon: 0.96, monsoon: 0.93, post-monsoon: 0.98, winter: 0.87, and annual: 0.94). Additionally, the SVM model exhibited substantial accuracy, as evidenced by consistently decreasing RMSE, MSE, and MAE values across all measurements.

Zone D (northwestern region) exhibited strong performance with the SVM model, as evidenced by a non-zero and non-negative R-squared value in Table 2. Low RMSE values (0.05 to 0.12) were also observed across all seasons (pre-monsoon, monsoon,

Table 2. Demonstrate the seasonal and annual ANN, SVM, and RF Model validation and testing outcome (bold colours are the significant predictive ET_0, and red colours values are insignificant values).

RMSE, R2, MSE and MAE Values of different models

			A						B					
			Pre-monsoon	Monsoon	Post-monsoon	Winter	Annual			Pre-monsoon	Monsoon	Post-monsoon	Winter	Annual
ANN	Training	RMSE	0.15	0.08	0.11	0.19	0.22	Training	RMSE	0.38	0.19	0.07	0.16	0.13
		R2	0.34	0.59	0.15	−1.21	−4.64		R2	−0.96	−0.01	0.84	0.28	0.22
		MSE	0.02	0.007	0.01	0.03	0.05		MSE	0.14	0.03	0.006	0.02	0.01
		MAE	0.1	0.06	0.08	0.13	0.1		MAE	0.15	0.12	0.05	0.12	0.1
	Testing	RMSE	0.64	0.09	0.38	0.73	1.82	Testing	RMSE	0.63	0.29	0.38	0.37	0.77
		R2	−2.51	0.78	−5.24	−11.08	−88.01		R2	−1.17	−1.15	−9.01	−1.91	−14.88
		MSE	0.04	0.008	0.14	0.53	3.31		MSE	0.4	0.08	0.14	0.14	0.6
		MAE	0.26	0.06	0.16	0.41	0.89		MAE	0.36	0.14	0.22	0.29	0.38
SVM	Training	RMSE	0.04	0.03	0.03	0.06	0.04	Training	RMSE	0.05	0.03	0.04	0.06	0.04
		R2	**0.95**	**0.92**	**0.91**	**0.77**	**0.8**		R2	**0.96**	**0.97**	**0.94**	**0.87**	**0.91**
		MSE	0	0.001	0.001	0.004	0.001		MSE	0.002	0.0009	0.002	0.004	0.001
		MAE	0.03	0.02	0.03	0.5	0.03		MAE	0.04	0.26	0.03	0.06	0.03
	Testing	RMSE	0.16	0.04	0.03	0.08	0.15	Testing	RMSE	0.07	0.01	0.03	0.11	0.05
		R2	**0.77**	**0.96**	**0.94**	**0.85**	0.38		R2	**0.97**	**0.99**	**0.91**	**0.74**	**0.91**
		MSE	0.03	0.001	0.001	0.006	0.02		MSE	0.005	0.0003	0.001	0.14	0.003
		MAE	0.1	0.03	0.03	0.05	0.11		MAE	0.04	0.01	0.02	0.08	0.04
RF	Training	RMSE	0.13	0.13	0.09	0.11	0.09	Training	RMSE	0.16	0.12	0.2	0.18	0.11
		R2	0.36	0	0.38	0.21	−0.06		R2	−0.57	0.61	−0.09	0.11	0.42
		MSE	0.01	0.01	0.009	0.01	0.009		MSE	0.02	0.014	0.04	0.03	0.01
		MAE	0.11	0.09	0.07	0.09	0.07		MAE	0.13	0.1	0.17	0.14	0.09
	Testing	RMSE	0.33	0.16	0.2	0.21	0.26	Testing	RMSE	0.37	0.22	0.15	0.21	0.19
		R2	0.01	0.24	−0.72	−0.04	−0.94		R2	0.26	−0.24	−0.73	0.04	−0.04
		MSE	0.11	0.02	0.04	0.04	0.07		MSE	0.13	0.04	0.02	0.04	0.03
		MAE	0.23	0.12	0.15	0.17	0.2		MAE	0.23	0.17	0.12	0.15	0.16
			C							D				
			Pre-monsoon	Monsoon	Post-monsoon	Winter	Annual			Pre-monsoon	Monsoon	Post-monsoon	Winter	Annual
ANN	Training	RMSE	0.08	0.18	0.01	0.44	0.2	Training	RMSE	0.38	0.09	0.07	0.18	0.12
		R2	**0.93**	**0.69**	**0.641**	−2.9	**0.86**		R2	−0.91	**0.67**	**0.71**	−0.54	0.02
		MSE	0.007	0.03	0.01	0.115	0.006		MSE	0.14	0.009	0.006	0.03	0.014
		MAE	0.06	0.14	0.096	0.25	0.06		MAE	0.2	0.05	0.06	0.14	0.09
	Testing	RMSE	0.1	0.35	0.01	0.44	0.2	Testing	RMSE	1.29	1.05	1.06	0.26	2.41
		R2	**0.92**	−0.51	**1**	−2.03	**0.55**		R2	−15.29	−28.43	−65.91	0.26	−288.7
		MSE	0.01	0.12	0.0002	0.19	0.04		MSE	1.67	1.1	1.12	0.06	5.81
		MAE	0.08	0.18	0.01	0.36	0.1		MAE	0.63	0.52	0.48	0.18	1.17
SVM	Training	RMSE	0.04	0.05	0.02	0.13	0.04	Training	RMSE	0.066	0.02	0.03	0.07	0.05
		R2	**0.98**	**0.97**	**0.98**	**0.42**	**0.95**		R2	**0.94**	**0.99**	**0.93**	**0.6**	**0.78**
		MSE	0.002	0.003	0.0006	0.017	0.002		MSE	0.004	0.004	0.001	0.01	0.003
		MAE	0.03	0.04	0.02	0.11	0.03		MAE	0.04	0.015	0.02	0.099	0.045
	Testing	RMSE	0.07	0.07	0.047	0.08	0.07	Testing	RMSE	0.05	0.04	0.09	0.12	0.09
		R2	**0.96**	**0.93**	**0.98**	**0.87**	**0.94**		R2	**0.97**	**0.94**	**0.44**	**0.6**	**0.55**
		MSE	0.005	0.006	0.0022	0.008	0.005		MSE	0.003	0.002	0.009	0.01	0.009
		MAE	0.07	0.04	0.03	0.06	0.04		MAE	0.04	0.04	0.05	0.099	0.05
RF	Training	RMSE	0.17	0.21	0.09	0.19	0.17	Training	RMSE	0.16	0.09	0.13	0.11	0.07
		R2	**0.74**	**0.58**	**0.78**	−0.26	**0.41**		R2	**0.63**	**0.71**	0.11	0.32	**0.58**
		MSE	0.03	0.04	0.008	0.03	0.02		MSE	0.02	0.008	0.018	0.014	0.006
		MAE	0.13	0.14	0.07	0.16	0.12		MAE	0.11	0.07	0.108	0.08	0.067
	Testing	RMSE	0.15	0.05	0.28	0.26	0.18	Testing	RMSE	0.26	0.15	0.22	0.18	0.12
		R2	**0.83**	**0.96**	0.111	−0.07	**0.62**		R2	0.32	**0.4**	−1.84	0.18	0.17
		MSE	0.02	0.002	0.08	0.068	0.03		MSE	0.06	0.02	0.048	0.03	0.016
		MAE	0.1	0.02	0.12	0.14	0.1		MAE	0.25	0.11	0.16	0.14	0.11
			E							F				
			Pre-monsoon	Monsoon	Post-monsoon	Winter	Annual			Pre-monsoon	Monsoon	Post-monsoon	Winter	Annual
ANN	Training	RMSE	0.24	0.17	0.09	0.17	0.2	Training	RMSE	0.17	0.2	0.21	0.2	0.24
		R2	**0.52**	0.1	**0.43**	−0.42	−0.74		R2	**0.61**	−0.6	−1.31	−0.69	−2.18
		MSE	0.05	0.03	0.009	0.03	0.04		MSE	0.03	0.04	0.04	0.04	0.05
		MAE	0.16	0.09	0.07	0.144	0.15		MAE	0.12	0.11	0.13	0.15	0.16
	Testing	RMSE	0.69	1.1	0.85	0.43	0.9	Testing	RMSE	0.79	0.81	0.28	0.3	1.34
		R2	−4.74	−23.27	−33.03	−7.18	−44.72		R2	−9.11	−13.56	−4.53	−1.46	−71.38
		MSE	0.47	1.22	0.72	0.18	0.81		MSE	0.63	0.64	0.08	0.09	1.79
		MAE	0.26	0.46	0.55	0.39	0.41		MAE	0.55	0.29	0.15	0.19	0.54
SVM	Training	RMSE	0.09	0.07	0.05	0.09	0.07	Training	RMSE	0.05	0.02	0.04	0.11	0.07
		R2	**0.92**	**0.83**	**0.79**	**0.63**	**0.77**		R2	**0.97**	**0.98**	**0.9**	**0.53**	0.005
		MSE	0.009	0.006	0.003	0.008	0.005		MSE	0.002	0.0005	0.002	0.01	0.005
		MAE	0.06	0.04	0.04	0.07	0.05		MAE	0.04	0.018	0.03	0.08	0.05
	Testing	RMSE	0.04	0.04	0.13	0.15	0.1	Testing	RMSE	0.06	0.03	0.04	0.15	0.06
		R2	**0.92**	**0.96**	0.19	−0.03	0.34		R2	**0.94**	**0.97**	**0.84**	**0.39**	**0.83**
		MSE	0.001	0.002	0.01	0.02	0.01		MSE	0.003	0.001	0.002	0.02	0.004
		MAE	0.03	0.03	0.08	0.13	0.07		MAE	0.04	0.02	0.03	0.13	0.04

(*Continued*)

Table 2. (Continued).

RF	Training	RMSE	0.29	0.12	0.48	0.11	0.15	Training	RMSE	0.21	0.1	0.14	0.13	0.11
		R2	0.3	**0.54**	**0.86**	**0.41**	−0.03		R2	**0.43**	**0.6**	0.01	0.31	0.25
		MSE	0.08	0.01	0.002	0.01	0.02		MSE	0.04	0.01	0.02	0.01	0.01
		MAE	0.21	0.1	0.03	0.09	0.11		MAE	0.18	0.07	0.12	0.11	0.1
	Testing	RMSE	0.34	0.16	0.11	0.21	0.2	Testing	RMSE	0.255	0.18	0.14	0.21	0.13
		R2	−0.44	**0.44**	**0.36**	−1.08	−1.84		R2	−0.04	0.25	−0.54	−0.14	0.31
		MSE	0.12	0.02	0.01	0.04	0.05		MSE	0.06	0.034	0.02	0.04	0.01
		MAE	0.28	0.14	0.07	0.16	0.2		MAE	0.22	0.11	0.13	0.15	0.12

G

			Pre-monsoon	Monsoon	Post-monsoon	Winter	Annual	RF		Pre-monsoon	Monsoon	Post-monsoon	Winter	Annual
ANN	Training	RMSE	0.29	0.39	0.21	0.25	0.24	Training	RMSE	0.14	0.11	0.085	0.15	0.08
		R2	−1.27	−7.48	−1.4	−2.86	−4.86		R2	**0.47**	0.25	**0.61**	−0.32	**0.37**
		MSE	0.08	0.15	0.04	0.06	0.06		MSE	0.019	0.013	0.007	0.02	0.006
		MAE	0.2	0.26	0.15	0.19	0.16		MAE	0.11	0.09	0.06	0.12	0.07
	Testing	RMSE	0.28	0.73	0.9	1.18	0.67	Testing	RMSE	0.3	0.2	0.28	0.33	0.22
		R2	0.26	−11.4	−20.45	−20.89	−9.12		R2	0.14	0	−1.08	−0.74	−0.18
		MSE	0.07	0.54	0.81	1.39	0.45		MSE	0.09	0.04	0.07	0.11	0.05
		MAE	0.22	0.41	0.54	0.8	0.34		MAE	0.19	0.18	0.21	0.25	0.17
SVM	Training	RMSE	0.09	0.06	0.05	0.1	0.07							
		R2	**0.78**	**0.8**	**0.81**	0.32	**0.47**							
		MSE	0.008	0.003	0.003	0.01	0.005							
		MAE	0.07	0.05	0.04	0.08	0.06							
	Testing	RMSE	0.2	0.16	0.08	0.11	0.14							
		R2	**0.6**	0.36	**0.83**	**0.78**	**0.56**							
		MSE	0.04	0.02	0.006	0.01	0.01							
		MAE	0.14	0.1	0.05	0.09	0.1							

post-monsoon, winter, and annual). Furthermore, relatively small MSE and MAE values supported the model's accuracy. These findings suggest potential increases in ET_0 values for the pre-monsoon, monsoon, winter, and annual seasons in upcoming years based on their respective R-squared values (0.97, 0.94, 0.60, and 0.55). Notably, the post-monsoon season is projected to experience a 44% increase in ET_0 fluctuation. These results align with the SVM model's effectiveness during validation, highlighting its suitability for Zone D. Conversely, the performance of the other two models was negligible, precluding their evaluation in this region.

In Zone E, denoting the western area, the RF method exhibited proficient performance during the monsoon and post-monsoon seasons, indicated by R-squared increases of 0.44 and 0.36 for ET_0, as shown in Table 2. Conversely, the RF model's predictive ability, particularly the ANN predictand value, was insignificant across all seasons – pre-monsoon, monsoon, post-monsoon, winter, and annual. The SVM model showcased notable enhancements in ET_0 for all seasons except winter, evidenced by R-squared values of 0.92, 0.96, 0.19, and 0.34 for pre-monsoon, monsoon, post-monsoon, and annual periods, respectively. Furthermore, the SVM model's accuracy is noteworthy, as evidenced by the consistent reductions observed in RMSE, MSE, and MAE values across measurements.

Zone F, representing the southwestern region, demonstrates notable SVM performance with non-zero and positive R^2 values, as outlined in Table 2. Additionally, the RMSE remains consistent at 0.06 across the pre-monsoon, monsoon, post-monsoon, and annual seasons, indicating strong model stability. The reduction in MSE and MAE values further highlights the model's high precision. As a result, ET_0 values are projected to increase significantly in the coming years, with anticipated growth rates of 94%, 97%, 84%, and 83% for the pre-monsoon, monsoon, post-monsoon, and annual seasons, respectively. Furthermore, the winter season is expected to see a considerable 39% rise in ET_0 variability. These findings align with the validation performance, underscoring the reliability and significance of the SVM model. In contrast, alternative approaches proved ineffective and unsuitable for evaluation within Zone F.

Zone G, encompassing the south-central region, witnessed robust SVM performance, surpassing expectations with diminished RMSE, MSE, and MAE values and avoiding 0 or negative r-squared values, as shown in Table 2. Specifically, SVM demonstrated RMSE values of 0.2, 0.16, 0.08, 0.11, and 0.14 for pre-monsoon, monsoon, post-monsoon, winter, and annual seasons. Furthermore, MSE (0.04, 0.02, 0.006, 0.1, and 0.01) and MAE (0.14, 0.1, 0.05, 0.09, and 0.1) values indicated reduced magnitudes across pre-monsoon, monsoon, post-monsoon, winter, and annual periods, underscoring the model's substantial accuracy. Consequently, future ET_0 variation projections suggest that the post-monsoon season will exhibit the most significant ET_0 increase over the coming decades, with an anticipated 83% climb. Additionally, substantial rises of approximately 60%, 78%, and 56% in ET_0 variance are foreseen for the pre-monsoon, winter, and annual seasons. These results align with

testing effectiveness, validating the SVM model's applicability. Conversely, the performance of the other two models remained marginal, precluding their recognition within Zone G. In a related manner (Ferreira et al., 2019), found that the SVM was the most robust alternate approach to the FAO56-PM. Also indicated that for estimating ET_0, SVM performed the best, with R2 values ranging from 0.882% to 0.993% (Wen et al., 2015). Based on precision, dependability, ease of use, and excellent correlation with ET_0's, the SVM model is the most appropriate approach for ET_0 prediction in Bangladesh. However, Salam, Islam, et al. (2020) found a different model of the Abtew (ET_0,6) model (Abtew, 1996) for the interannual and multiyear ET_0 prediction.

Table 3 presents correlation coefficients between various climate variables, seasons, and geographic zones predicting the ET_0. It reveals several notable patterns, as strong positive correlations exist between maximum temperature and wind speed across most zones and seasons, suggesting a linked relationship like most dependent in predicting the ET_0. Rainfall shows weak to moderate negative correlations with maximum temperature, wind speed, and sunshine hours, indicating inverse relationships. Humidity generally has moderate to strong positive correlations with wind speed, especially in Zones C, D, and G, hinting at potential connections. Zone B stands out with consistently high correlations between maximum temperature and wind speed, suggesting a robust association in that region. Zone C exhibits distinct patterns with weaker correlations between temperature and wind and even positive correlations between rainfall and temperature in some seasons, implying unique climate dynamics. These correlations offer insights into the interplay of climate variables

The nation's agricultural output is expected to suffer due to increasing ET_0 trends in the coming years (Kousari & Ahani, 2012; Rahman et al., 2019) It has been observed that the FAO Penman-Monteith method is more accurate in estimating ET_0, while various machine learning techniques are highly effective at predicting it (Ikram et al., 2023; Kumari et al., 2022). Boro rice, known as dry season rice, is an essential staple for Bangladesh's vast population. It plays a crucial role in the country's economy and is cultivated nationwide. However, this grain crop heavily relies on copious water supply during all its growth phases, from soil preparation to grain harvesting. The cultivation period for Boro rice spans from November to April, and irrigation is a must during this period. Bangladesh faces challenges such as limited rainfall, and drought episodes can further exacerbate the situation. In such circumstances, the water supply becomes scarce, significantly impacting the crop yield and the country's overall economy (Rahman & Azim, 2021b). Consequently, the escalating ET_0 trend adds complexity to the predicament faced by various water-dependent industries. Farmers may extract additional water from subsurface sources in this evolving scenario. However, groundwater quality has deteriorated since the 1980s (Salam, Islam, et al., 2020). While precipitation projections indicate a rise in national precipitation in the 21st century, groundwater

Table 3. Correlation coefficient analysis.

Variables	Season	Zone A	Zone B	Zone C	Zone D	Zone E	Zone F	Zone G
Max temp	Pre-monsoon	0.69	0.84	−0.04	0.61	0.52	0.55	0.70
	Monsoon	0.69	0.68	−0.21	0.53	0.52	0.56	0.66
	Post-monsoon	0.75	0.70	0.07	0.53	0.46	0.58	0.74
	Winter	0.67	0.76	0.13	0.73	0.52	0.52	0.68
	Annual	0.70	0.73	−0.08	0.47	0.28	0.40	0.72
Min Temp	Pre-monsoon	−0.18	−0.01	0.17	−0.07	−0.01	0.12	−0.21
	Monsoon	−0.14	0.09	−0.03	−0.30	−0.22	−0.14	−0.18
	Post-monsoon	0.03	0.11	0.05	0.02	0.13	−0.10	0.04
	Winter	−0.57	−0.04	−0.29	−0.44	−0.38	−0.56	−0.37
	Annual	−0.40	−0.07	−0.06	−0.50	−0.37	−0.39	−0.42
Rainfall	Pre-monsoon	−0.54	−0.44	0.02	−0.55	−0.50	−0.43	−0.48
	Monsoon	−0.61	−0.36	−0.12	−0.54	−0.36	−0.54	−0.54
	Post-monsoon	−0.25	−0.32	0.41	−0.45	−0.49	−0.63	−0.45
	Winter	−0.37	−0.14	−0.04	−0.06	0.15	−0.09	0.12
	Annual	−0.29	−0.23	0.27	−0.23	−0.38	−0.46	−0.35
Humidity	Pre-monsoon	−0.83	−0.82	−0.36	−0.85	−0.80	−0.59	−0.76
	Monsoon	−0.79	−0.76	0.15	−0.58	−0.61	−0.63	−0.84
	Post-monsoon	−0.26	−0.39	−0.25	−0.65	−0.21	−0.62	−0.54
	Winter	−0.17	0.11	−0.01	−0.37	−0.19	−0.37	−0.12
	Annual	−0.60	−0.49	−0.26	−0.70	−0.47	−0.58	−0.62
Wind	Pre-monsoon	0.59	0.63	0.76	0.63	0.55	0.69	0.72
	Monsoon	0.17	0.33	0.73	0.29	0.14	0.33	0.40
	Post-monsoon	0.56	0.61	0.84	0.60	0.35	0.58	0.75
	Winter	0.71	0.75	0.82	0.25	0.28	0.55	0.77
	Annual	0.70	0.77	0.82	0.59	0.56	0.74	0.80
Sunshine hour	Pre-monsoon	0.61	0.52	0.10	0.62	0.56	0.38	0.31
	Monsoon	0.82	0.79	0.34	0.81	0.86	0.79	0.74
	Post-monsoon	0.59	0.65	−0.19	0.51	0.63	0.54	0.26
	Winter	0.10	0.03	−0.13	0.46	0.50	0.39	−0.13
	Annual	0.33	0.12	0.11	0.39	0.45	0.33	−0.06

recharge is influenced by more than just precipitation. The transboundary water crisis significantly impacts groundwater replenishment, agriculture, fisheries, and national navigation (Biswas, 2011).

As the levels of ET_0, or evapotranspiration, increase, it poses a significant challenge for farmers as it leads to increased irrigation costs, which can harm their productivity. Additionally, other water-intensive industries such as manufacturing and construction, will also be affected, as there is a growing concern about the environmental and public health implications of excessive water usage. In addition, changes in ET_0 levels can significantly impact various hydrological processes, including soil moisture levels, groundwater extraction, and runoff, which can have far-reaching consequences for the environment and ecosystems (Jerin et al., 2021). For instance, flooding adversely impacts the progress of infrastructure development, network systems, academic and administrative institutions, and tangible assets (Kabir & Hossen, 2019). To address the country's climatic variability and ET_0 consequences, potential strategies include exploring alternative uses of groundwater for irrigation, constructing reservoirs to retain monsoon water, and adopting suitable irrigation frameworks.

4. Conclusion

In conclusion, this study has comprehensively analyzed ET_0 trends, magnitudes, and predictions in Bangladesh. The findings highlight the exceptional predictive capabilities of the SVM model in forecasting patterns, outperforming the ANN and RF models in various zones.

(1) For Zone A, SVM-based predictions indicate an expected increase in ET_0 values in the coming years, particularly during the monsoon, post-monsoon, and winter seasons, with positive prediction values of 96%, 94%, and 85%, respectively. Higher temperatures, monsoon humidity, and reduced winter cloud cover contribute to the increase.
(2) Similarly, Zone B is projected to experience elevated ET_0 levels across all seasons, with prediction values of 97%, 99%, 91%, 74%, and 91% for pre-monsoon, monsoon, post-monsoon, winter, and annual periods, respectively. Zone B's climate, characterized by high temperatures, strong solar radiation, and variable humidity, drives this trend.
(3) Zone C is expected to significantly rise ET_0 during all seasons, as reflected by the respective R-squared values of 0.96, 0.93, 0.98, 0.87, and 0.94. Increasing temperatures, variable rainfall, and higher wind speeds contribute to the rise.
(4) In Zone D, the pre-monsoon, monsoon, winter, and annual seasons are anticipated to have higher ET_0 values in the coming years, with R-squared values of 0.97, 0.94, 0.6, and 0.55, respectively. Elevated pre-monsoon and monsoon temperatures, lower winter humidity, and higher solar radiation influence these predictions.
(5) For Zone E, an increase in ET_0 is projected for all seasons except winter, with R-squared values of 0.92, 0.96, 0.19, and 0.34 for pre-monsoon, monsoon, post-monsoon, and annual periods, respectively. Lower winter temperatures and higher humidity likely contribute to the lower ET_0 prediction for that season.
(6) Similarly, this study's predictions suggest that Zone F's pre-monsoon, monsoon, post-monsoon, and annual seasons will experience increased ET_0 in the following years F, with projection values of 94%, 97%, 84%, and 83%, respectively. Zone F's climate, characterized by high temperatures, intense solar radiation, and seasonal winds, contributes to the rise.

The study reveals that combining prediction outcomes, historical trends, and magnitude assessments can significantly inform irrigation practices in Bangladesh. Highlighting the need for prudent water resource management, this research addresses challenges posed by climate change and ET_0 fluctuations across the country's seven climatic zones. The insights offer a foundation for policy development, urging policymakers to adopt sustainable approaches for water resource resilience. The study's recommendations emphasize sustainable practices as key to long-term water sustainability. The government and stakeholders must collaborate on water management policies grounded in scientific evidence and practical experience, ensuring both immediate alleviation of challenges and safeguarding future water needs in Bangladesh.

Abbreviations

ET_0	Reference Evapotranspiration
ANN	Artificial Neural Network
SVM	Support Vector Machine
RF	Random Forest
SR	Solar radiation
SD	Sunshine duration
IDW	Inverse Distance Weighting
MMK	Modified Mann Kendall
MSE	Mean square error
MAE	Mean absolute error
RMSE	Root mean square error

Disclosure statement

No potential conflict of interest was reported by the author(s).

ORCID

Md. Naimur Rahman http://orcid.org/0000-0001-5236-3784

Data availability statement

Data will be made available upon request.

References

Abtew, W. (1996). Evapotranspiration measurements and modeling for three wetland systems in south Florida 1. *JAWRA Journal of the American Water Resources Association*, *32*(3), 465–473. https://doi.org/10.1111/j.1752-1688.1996.tb04044.x

Ahmad, M. J., Cho, G.-H., Kim, S.-H., Lee, S., Adelodun, B., & Choi, K.-S. (2021). Influence mechanism of climate change over crop growth and water demands for wheat-rice system of Punjab, Pakistan. *Journal of Water and Climate Change*, *12*(4), 1184–1202. https://doi.org/10.2166/wcc.2020.009

Alexandersson, H. (1986). A homogeneity test applied to precipitation data. *Journal of Climatology*, *6*(6), 661–675. https://doi.org/10.1002/joc.3370060607

Allen, R. G., Pereira, L. S., Raes, D., Smith, M., & A B W. (1998). *Crop evapotranspiration - guidelines for computing crop water requirements - FAO irrigation and drainage paper 56. Irrigation and drainage*. https://doi.org/10.1016/j.eja.2010.12.001

Amini, M. A., Torkan, G., Eslamian, S., Zareian, M. J., & Adamowski, J. F. (2019). Analysis of deterministic and geostatistical interpolation techniques for mapping meteorological variables at large watershed scales. *Acta Geophysica*, *67*(1), 275–275. https://doi.org/10.1007/s11600-018-0235-x

Ashraf, H., Qamar, S., Riaz, N., Shamshiri, R. R., Sultan, M., Khalid, B., Ibrahim, S. M., Imran, M., & Khan, M. U. (2023). Spatiotemporal Estimation of Reference Evapotranspiration for Agricultural Applications in Punjab, Pakistan. *Agriculture*, *13*(7), 1388. https://doi.org/10.3390/agriculture13071388

Azid, A., Juahir, H., Latif, M. T., Zain, S. M., Osman, M. R., Azid, A., Juahir, H., Latif, M. T., Zain, S. M., & Osman, M. R. (2013). Feed-forward artificial neural network model for air pollutant index prediction in the southern region of Peninsular Malaysia. *Journal of Environmental Protection*, *4*(12), 1–10. https://doi.org/10.4236/JEP.2013.412A1001

Azid, A., Juahir, H., Toriman, M. E., Kamarudin, M. K. A., Saudi, A. S. M., Hasnam, C. N. C., Aziz, N. A. A., Azaman, F., Latif, M. T., Zainuddin, S. F. M., Osman, M. R., & Yamin, M. (2014). Prediction of the level of air pollution using principal component analysis and artificial neural network techniques: A case study in Malaysia. *Water, Air, and Soil Pollution*, *225*(8), 1–14. https://doi.org/10.1007/s11270-014-2063-1

Baruah, U. D., Saikia, A., & Mili, N. (2023). Modelling of reference crop evapotranspiration in humid-wet tropical region of India. In S. Sharma, J. C. Kuniyal, P. Chand & P. Singh (Eds.), *Climate change adaptation, risk management and sustainable practices in the Himalaya* (pp. 407–417). Springer. https://doi.org/10.1007/978-3-031-24659-3_17.

Batchelor, C. H., & Roberts, J. (1983). Evaporation from the irrigation water, foliage and panicles of paddy rice in north-east Sri Lanka. *Agricultural Meteorology*, *29*(1), 11–26. https://doi.org/10.1016/0002-1571(83)90072-9

Behboudian, M., Kerachian, R., Motlaghzadeh, K., & Ashrafi, S. (2021). Evaluating water resources management scenarios considering the hierarchical structure of decision-makers and ecosystem services-based criteria. *Science of the Total Environment*, *751*, 141759. https://doi.org/10.1016/j.scitotenv.2020.141759

Bernadette, I. C., Moses, A. O., & Martin, I. O. (2014). Evaluation of evapotranspiration using FAO penman-monteith method in Kano Nigeria. *International Journal of Science and Technology*, *3*(11), 698–703. https://scholar.google.com/citations?view_op=view_citation&hl=en&user=t6VSHxaeLV0C&citation_for_view=t6VSHxaeLV0C:4TOpqqG69KYC

Biazar, S. M., Dinpashoh, Y., & Singh, V. P. (2019). Sensitivity analysis of the reference crop evapotranspiration in a humid region. *Environmental Science and Pollution Research*, *26*(31), 32517–32544. https://doi.org/10.1007/s11356-019-06419-w

Biswas, A. K. (2011). Cooperation or conflict in transboundary water management: Case study of South Asia. *Hydrological Sciences Journal*, *56*(4), 662–670. https://doi.org/10.1080/02626667.2011.572886

Breiman, L. (2001). Random forests. *Machine Learning*, *45*(1), 5–32. https://doi.org/10.1023/A:1010933404324

Buishand, T. A. (1982). Some methods for testing the homogeneity of rainfall records. *Journal of Hydrology*, *58*(1), 11–27. https://doi.org/10.1016/0022-1694(82)90066-X

Cabral Júnior, J. B., Silva, C. M. S. E., de Almeida, H. A., Bezerra, B. G., & Spyrides, M. H. C. (2019). Detecting linear trend of reference evapotranspiration in irrigated farming areas in Brazil's semiarid region. *Theoretical and Applied Climatology*, *138*(1–2), 215–225. https://doi.org/10.1007/s00704-019-02816-w

Chaloulakou, A., Grivas, G., & Spyrellis, N. (2003). Neural network and multiple regression models for PM10 prediction in Athens: A comparative assessment. *Journal of the Air & Waste Management Association*, *53*(10), 1183–1190. https://doi.org/10.1080/10473289.2003.10466276

Chen, J., Zhang, J., Peng, J., Zou, L., Fan, Y., Yang, F., & Hu, Z. (2023). Alp-valley and elevation effects on the reference evapotranspiration and the dominant climate controls in Red River Basin, China: Insights from geographical differentiation. *Journal of Hydrology*, *620*, 129397. https://doi.org/10.1016/j.jhydrol.2023.129397

Cheshmberah, F., & Zolfaghari, A. A. (2019). The effect of climate change on future reference evapotranspiration in different climatic zones of Iran. *Pure & Applied Geophysics*, *176*(8), 3649–3664. https://doi.org/10.1007/s00024-019-02148-w

Dai, A. (2021). Hydroclimatic trends during 1950–2018 over global land. *Climate Dynamics*, *56*(11–12), 4027–4049. https://doi.org/10.1007/s00382-021-05684-1

Das, S. (2019). Extreme rainfall estimation at ungauged sites: Comparison between region-of-influence approach of regional analysis and spatial interpolation technique. *International Journal of Climatology*, *39*(1), 407–423. https://doi.org/10.1002/joc.5819

Dinpashoh, Y., & Babamiri, O. (2020). Trends in reference crop evapotranspiration in Urmia Lake basin. *Arabian*

Journal of Geosciences, *13*(10), 1–16. https://doi.org/10.1007/s12517-020-05404-9

Dong, Q., Wang, W., Shao, Q., Xing, W., Ding, Y., & Fu, J. (2020). The response of reference evapotranspiration to climate change in Xinjiang, China: Historical changes, driving forces, and future projections. *International Journal of Climatology*, *40*(1), 235–254. https://doi.org/10.1002/joc.6206

Elbeltagi, A., Kumari, N., Dharpure, J. K., Mokhtar, A., Alsafadi, K., Kumar, M., Mehdinejadiani, B., Ramezani Etedali, H., Brouziyne, Y., Towfiqul Islam, A. R. M., & Kuriqi, A. (2021). Prediction of combined terrestrial evapotranspiration index (CTEI) over Large River Basin Based on machine learning approaches. *Water*, *13*(4), e547. https://doi.org/10.3390/W13040547

Fan, J., Ma, X., Wu, L., Zhang, F., Yu, X., & Zeng, W. (2019). Light gradient boosting machine: An efficient soft computing model for estimating daily reference evapotranspiration with local and external meteorological data. *Agricultural Water Management*, *225*, 105758. https://doi.org/10.1016/j.agwat.2019.105758

FAO. (2024). *FAO penman-monteith equation*. FAO Penman-Monteith Equation. https://www.fao.org/3/x0490e/x0490e06.htm

Ferreira, L. B., da Cunha, F. F., de Oliveira, R. A., & Fernandes Filho, E. I. (2019). Estimation of reference evapotranspiration in Brazil with limited meteorological data using ANN and SVM–A new approach. *Journal of Hydrology*, *572*, 556–570. https://doi.org/10.1016/j.jhydrol.2019.03.028

Ferreira, L. B., da Cunha, F. F., & Fernandes Filho, E. I. (2022). Exploring machine learning and multi-task learning to estimate meteorological data and reference evapotranspiration across Brazil. *Agricultural Water Management*, *259*, 107281. https://doi.org/10.1016/j.agwat.2021.107281

Fu, J., Gong, Y., Zheng, W., Zou, J., Zhang, M., Zhang, Z., Qin, J., Liu, J., & Quan, B. (2022). Spatial-temporal variations of terrestrial evapotranspiration across China from 2000 to 2019. *Science of the Total Environment*, *825*, 153951. https://doi.org/10.1016/j.scitotenv.2022.153951

Heramb, P., Ramana Rao, K. V., Subeesh, A., & Srivastava, A. (2023). Predictive modelling of reference evapotranspiration using machine learning models coupled with Grey Wolf Optimizer. *Water (Switzerland)*, *15*(5), 856. https://doi.org/10.3390/w15050856

Hodam, S., Sarkar, S., Marak, A. G. R., Bandyopadhyay, A., & Bhadra, A. (2017). Spatial interpolation of reference evapotranspiration in India: Comparison of IDW and Kriging methods. *Journal of the Institution of Engineers (India): Series A*, *98*(4), 511–524. https://doi.org/10.1007/s40030-017-0241-z

Hwang, J. H., Azam, M., Jin, M. S., Kang, Y. H., Lee, J. E., Latif, M., Ahmed, R., Umar, M., & Hashmi, M. Z. (2020). Spatiotemporal trends in reference evapotranspiration over South Korea. *Paddy and Water Environment*, *18*(1), 235–259. https://doi.org/10.1007/s10333-019-00777-4

Ikram, R. M. A., Mostafa, R. R., Chen, Z., Islam, A. R. M. T., Kisi, O., Kuriqi, A., & Zounemat-Kermani, M. (2023). Advanced hybrid metaheuristic machine learning models application for reference crop evapotranspiration prediction. *Agronomy*, *13*(1), 98. https://doi.org/10.3390/agronomy13010098

Jerin, J. N., Islam, H. M. T., Islam, A. R. M. T., Shahid, S., Hu, Z., Badhan, M. A., Chu, R., & Elbeltagi, A. (2021). Spatiotemporal trends in reference evapotranspiration and its driving factors in Bangladesh. *Theoretical and Applied Climatology*, *144*(1), 793–808. https://doi.org/10.1007/s00704-021-03566-4

Jung, M., Reichstein, M., Ciais, P., Seneviratne, S. I., Sheffield, J., Goulden, M. L., Bonan, G., Cescatti, A., Chen, J., De Jeu, R., Dolman, A. J., Eugster, W., Gerten, D., Gianelle, D., Gobron, N., Heinke, J., Kimball, J., Law, B. E. . . . Zaehle, S. (2010). Recent decline in the global land evapotranspiration trend due to limited moisture supply. *Nature*, *467*(7318), 951–954. https://doi.org/10.1038/nature09396

Kabir, M. H., & Hossen, M. N. (2019). Impacts of flood and its possible solution in Bangladesh. *Disaster Advances*, *12*(10), 48–57.

Kamal, A. S. M., Hossain, F., & Shahid, S. (2021). Spatiotemporal changes in rainfall and droughts of Bangladesh for 1. 5 and 2° C temperature rise scenarios of CMIP6 models. *Theoretical and Applied Climatology*, *146*(1), 527–542. https://doi.org/10.1007/s00704-021-03735-5

Kamruzzaman, M., Hwang, S., Cho, J., Jang, M. W., & Jeong, H. (2019). Evaluating the spatiotemporal characteristics of agricultural drought in Bangladesh using effective drought index. *Water*, *11*(12), 2437. https://doi.org/10.3390/W11122437

Katerji, N., & Rana, G. (2011). Crop reference evapotranspiration: A discussion of the concept, analysis of the process and validation. *Water Resources Management*, *25*(6), 1581–1600. https://doi.org/10.1007/s11269-010-9762-1

Kendall, M. G. (1975). *Rank correlation methods* (4th ed.). Oxford University Press.

Kitsara, G., Papaioannou, G., Papathanasiou, A., & Retalis, A. (2013). Dimming/Brightening in Athens: Trends in sunshine duration, cloud cover and reference evapotranspiration. *Water Resources Management*, *27*(6), 1623–1633. https://doi.org/10.1007/s11269-012-0229-4

Kousari, M. R., & Ahani, H. (2012). An investigation on reference crop evapotranspiration trend from 1975 to 2005 in Iran. *International Journal of Climatology*, *32*(15), 2387–2402. https://doi.org/10.1002/joc.3404

Kumari, A., Upadhyaya, A., Jeet, P., Al-Ansari, N., Rajput, J., Sundaram, P. K., Saurabh, K., Prakash, V., Singh, A. K., Raman, R. K., Gaddikeri, V., & Kuriqi, A. (2022). Estimation of actual evapotranspiration and crop coefficient of transplanted puddled rice using a modified non-weighing Paddy Lysimeter. *Agronomy*, *12*(11), e2850. https://doi.org/10.3390/AGRONOMY12112850

Li, M., Chu, R., Shen, S., & Islam, A. R. M. (2018). Quantifying climatic impact on reference evapotranspiration trends in the Huai River Basin of eastern China. *Water*, *10*(2), 144. https://doi.org/10.3390/w10020144

Lin, P., He, Z., Du, J., Chen, L., Zhu, X., & Li, J. (2018). Impacts of climate change on reference evapotranspiration in the Qilian Mountains of China: Historical trends and projected changes. *International Journal of Climatology*, *38*(7), 2980–2993. https://doi.org/10.1002/joc.5477

Mainuddin, M., Kirby, M., Chowdhury, R. A. R., & Shah-Newaz, S. M. (2015). Spatial and temporal variations of, and the impact of climate change on, the dry season crop irrigation requirements in Bangladesh. *Irrigation Science*, *33*(2), 107–120. https://doi.org/10.1007/s00271-014-0451-3

Mann, H. B. (1945). Nonparametric tests against trend. *Econometrica*, *13*(3), 245. https://doi.org/10.2307/1907187

Mao, K., Yuan, Z., Zuo, Z., Xu, T., Shen, X., & Gao, C. (2019). Changes in global cloud cover based on remote sensing data from 2003 to 2012. *Chinese Geographical Science*, *29*(2), 306–315. https://doi.org/10.1007/s11769-019-1030-6

Matuszko, D. (2012). Influence of the extent and genera of cloud cover on solar radiation intensity. *International Journal of Climatology*, *32*(15), 2403–2414. https://doi.org/10.1002/joc.2432

McEvoy, D. J., Pierce, D. W., Kalansky, J. F., Cayan, D. R., & Abatzoglou, J. T. (2020). Projected changes in reference evapotranspiration in California and Nevada: Implications for drought and wildland fire danger. *Earth's Future*, *8*(11), e2020EF001736. https://doi.org/10.1029/2020EF001736

Meris, P. R., Dimaunahan, E., Dela Cruz, J. C., Fadchar, N. A., Manuel, M. C., Bonaobra, J. C. C., Ranosa, F. J. I., Mangaoang, J. L. D., & Reyes, P. C. (2020). IOT based - automated indoor air quality and LPG leak detection control system using support vector machine. *2020 11th IEEE Control and System Graduate Research Colloquium, ICSGRC 2020 - Proceedings*, Shah Alam, Malaysia (pp. 231–235). https://doi.org/10.1109/ICSGRC49013.2020.9232472.

Mishra, A. K. (2019). Investigating changes in cloud cover using the long-term record of precipitation extremes. *Meteorological Applications*, *26*(1), 108–116. https://doi.org/10.1002/met.1745

Mortuza, M. R., Moges, E., Demissie, Y., & Li, H. Y. (2019). Historical and future drought in Bangladesh using copula-based bivariate regional frequency analysis. *Theoretical and Applied Climatology*, *135*(3–4), 855–871. https://doi.org/10.1007/s00704-018-2407-7

Moustris, K. P., Ziomas, I. C., & Paliatsos, A. G. (2010). 3-day-ahead forecasting of regional pollution index for the pollutants NO2, CO, SO2, and O3 using artificial neural networks in Athens, Greece. *Water, Air, and Soil Pollution*, *209*(1–4), 29–43. https://doi.org/10.1007/s11270-009-0179-5

Ndiaye, P. M., Bodian, A., Diop, L., Deme, A., Dezetter, A., Djaman, K., & Ogilvie, A. (2020). Trend and sensitivity analysis of reference evapotranspiration in the Senegal river basin using NASA meteorological data. *Water*, *12*(7), 1957. https://doi.org/10.3390/w12071957

Ozelkan, E., Bagis, S., Ozelkan, E. C., Ustundag, B. B., Yucel, M., & Ormeci, C. (2015). Spatial interpolation of climatic variables using land surface temperature and modified inverse distance weighting. *International Journal of Remote Sensing*, *36*(4), 1000–1025. https://doi.org/10.1080/01431161.2015.1007248

Pereira, L. S., Paredes, P., & Jovanovic, N. (2020). Soil water balance models for determining crop water and irrigation requirements and irrigation scheduling focusing on the FAO56 method and the dual kc approach. *Agricultural Water Management*, *241*, 106357. https://doi.org/10.1016/j.agwat.2020.106357

Pour, S. H., Wahab, A. K. A., Shahid, S., & Ismail, Z. B. (2020). Changes in reference evapotranspiration and its driving factors in Peninsular Malaysia. *Atmospheric Research*, *246*, 105096. https://doi.org/10.1016/j.atmosres.2020.105096

Quej, V. H., Almorox, J., Arnaldo, J. A., & Moratiel, R. (2019). Evaluation of temperature-based methods for the estimation of reference evapotranspiration in the Yucatán peninsula, Mexico. *Journal of Hydrologic Engineering*, *24*(2), 5018029. https://doi.org/10.1061/(ASCE)HE.1943-5584.0001747

Rahman, M. A., Yunsheng, L., Sultana, N., & Ongoma, V. (2019). Analysis of reference evapotranspiration (ET0) trends under climate change in Bangladesh using observed and CMIP5 data sets. *Meteorology and Atmospheric Physics*, *131*(3), 639–655. https://doi.org/10.1007/s00703-018-0596-3

Rahman, M. N., Anowerul, S., Akter, F., Hasan, R., Ahmad, B., & Rouf, A. (2023). Quantification of rainfall, temperature, and reference evapotranspiration trend and their interrelationship in sub-climatic zones of Bangladesh. *Heliyon Elsevier*, *9*(9), e19559. https://doi.org/10.1016/j.heliyon.2023.e19559

Rahman, M. N., & Azim, S. A. (2021a). Meteorological drought in Bangladesh using standardized precipitation index: A spatiotemporal approach. *The Dhaka University Journal of Earth and Environmental Sciences*, *10*(3), 1–16. https://doi.org/10.3329/dujees.v10i3.59067

Rahman, M. N., & Azim, S. A. (2021b). Spatiotemporal evaluation of rainfall trend during 1979-2019 in seven climatic zones of Bangladesh. *Geology, Ecology & Landscapes*, *7*(4), 340–355. https://doi.org/10.1080/24749508.2021.2022425

Rahman, M., Rony, N., Md, R. H., & Jannat, F. A. (2021). Spatiotemporal evaluation of drought trend during 1979–2019 in seven climatic zones of Bangladesh. *Heliyon Elsevier*, *7*(11), e08249. https://doi.org/10.1016/j.heliyon.2021.e08249

Rajput, J., Singh, M., Lal, K., Khanna, M., Sarangi, A., Mukherjee, J., & Singh, S. (2024). Data-driven reference evapotranspiration (ET0) estimation: A comparative study of regression and machine learning techniques. *Environment, Development, and Sustainability*, *26*(5), 12679–12706. https://doi.org/10.1007/s10668-023-03978-4

Ramachandra, J. T., Veerappa, S. R. N., & Udupi, D. A. (2022). Assessment of spatiotemporal variability and trend analysis of reference crop evapotranspiration for the southern region of Peninsular India. *Environmental Science and Pollution Research*, *29*(28), 41953–41970. https://doi.org/10.1007/s11356-021-15958-0

Sahoo, B., Walling, I., Deka, B. C., & Bhatt, B. P. (2012). Standardization of reference evapotranspiration models for a subhumid valley rangeland in the Eastern Himalayas. *Journal of Irrigation & Drainage Engineering*, *138*(10), 880–895. https://doi.org/10.1061/(ASCE)IR.1943-4774.0000476

Salam, R., & Islam, A. R. M. T. (2020). Potential of RT, bagging and RS ensemble learning algorithms for reference evapotranspiration prediction using climatic data-limited humid region in Bangladesh. In *Journal of hydrology* (Vol. 590). Elsevier B.V. https://doi.org/10.1016/j.jhydrol.2020.125241

Salam, R., Islam, A. R. M. T., Pham, Q. B., Dehghani, M., Al-Ansari, N., & Linh, N. T. T. (2020). The optimal alternative for quantifying reference evapotranspiration in climatic sub-regions of Bangladesh. *Scientific Reports*, *10*(1), 20171. https://doi.org/10.1038/s41598-020-77183-y

Salam, R., Towfiqul Islam, A. R. M., & Islam, S. (2020). Spatiotemporal distribution and prediction of groundwater level linked to ENSO teleconnection indices in the northwestern region of Bangladesh. *Environment, Development, and Sustainability*, *22*(5), 4509–4535. https://doi.org/10.1007/s10668-019-00395-4

Sen, P. K. (1968). Estimates of the regression coefficient based on Kendall's tau. *Journal of the American Statistical Association*, *63*(324). https://doi.org/10.1080/01621459.1968.10480934

Srivastava, A., Sahoo, B., Raghuwanshi, N. S., & Chatterjee, C. (2018). Modelling the dynamics of evapotranspiration using variable infiltration capacity model and regionally calibrated Hargreaves approach. *Irrigation Science*, *36*(4–5), 289–300. https://doi.org/10.1007/s00271-018-0583-y

Wang, X., Liu, H., Zhang, L., & Zhang, R. (2014). Climate change trend and its effects on reference evapotranspiration at Linhe Station, Hetao Irrigation District. *Water Science & Engineering*, *7*(3), 250–266.

Wang, Z., Xie, P., Lai, C., Chen, X., Wu, X., Zeng, Z., & Li, J. (2017). Spatiotemporal variability of reference evapotranspiration and contributing climatic factors in China during 1961–2013. *Journal of Hydrology*, *544*, 97–108. https://doi.org/10.1016/j.jhydrol.2016.11.021

Wen, X., Si, J., He, Z., Wu, J., Shao, H., & Yu, H. (2015). Support-vector-machine-based models for modeling daily reference evapotranspiration with limited climatic data in extreme arid regions. *Water Resources Management*, *29*(9), 3195–3209. https://doi.org/10.1007/s11269-015-0990-2

Xing, W., Wang, W., Shao, Q., Yu, Z., Yang, T., & Fu, J. (2016). Periodic fluctuation of reference evapotranspiration during the past five decades: Does evaporation paradox really exist in China? *Scientific Reports*, *6*(1), 1–12. https://doi.org/10.1038/srep39503

Yassen, A. N., Nam, W.-H., & Hong, E.-M. (2020). Impact of climate change on reference evapotranspiration in Egypt. *Catena*, *194*, 104711. https://doi.org/10.1016/j.catena.2020.104711

Zhang, X., Wang, L., & Chen, D. (2019). How does temporal trend of reference evapotranspiration over the Tibetan plateau change with elevation? *International Journal of Climatology*, *39*(4), 2295–2305. https://doi.org/10.1002/joc.5951